(29) S. G. Pyke and R. G. Linck, *J. Am. Chem. Soc.*, **93**, 5281 (1971).
(30) M. T. Gandolfi, M. F. Manfrin, A. Juris, L. Moggi, and V. Balzani, *Inorg. Chem.*, **13**, 1342 (1974).
(31) M. Wrighton and D. Bredesen, *Inorg. Chem.*, **12**, 1707 (1973).
(32) L. Viaene, J. D'Olieslager, and S. De Jaegere, *Bull. Soc. Chim. Belg.*, **83**, 31 (1974).
(33) L. Viaene, Doctoral Thesis, Louvain 1975.
(34) R. A. Pribush, C. K. Poon, C. M. Bruce, and A. W. Adamson, *J. Am. Chem. Soc.*, **96**, 3027 (1974).
(35) H. Gafney and A. W. Adamson, *Coord. Chem. Rev.*, **16**, 171 (1975).
(36) P. S. Sheridan and A. W. Adamson, *J. Am. Chem. Soc.*, **96**, 3032 (1974).
(37) P. C. Ford, J. D. Petersen, and R. E. Hintze, *Coord. Chem. Rev.*, **14**, 67 (1974).
(38) M. Wrighton, *Chem. Rev.*, **74**, 401 (1974).
(39) A. D. Kirk, K. C. Moss, and J. G. Valentin, *Can. J. Chem.*, **49**, 1524 (1971).
(40) C. H. Langford and C. P. J. Vuik, *J. Am. Chem. Soc.*, **98**, 5409 (1976).

Kinetics of the Electron-Transfer Reactions of Azaviolene Radical Ions. 2.[1] Correlation with the Marcus Theory. The Question of Concerted Acid–Base Catalysis

Claude F. Bernasconi* and Hsien-chang Wang

Contribution from the Thimann Laboratories of the University of California, Santa Cruz, California 95064. *Received August 31, 1976*

Abstract: The comproportionation–disproportionation kinetics of the azaviolene redox systems derived from 1-ethyl-2-quinolone azine (I), 1-ethyl-2-pyridone azine (III), and 1,3-dimethyl-2-benzimidazolone azine (IV) have been studied in 50% acetonitrile–50% water (v/v), IV also in 50% 2-methoxyethanol–50% water (v/v), by temperature-jump, stopped-flow, and pH-jump techniques. Electron transfer was found to occur by three concurrent pathways, viz., (1) Red + $Ox^{2+} \rightleftarrows Sem^+ + Sem^+$, (2) $RedH^+ + Ox^{2+} \rightleftarrows Sem^+ + SemH^{2+}$, and (3) a concerted general acid–base catalyzed reaction $RedH^+ + Ox^{2+} + B^- \rightleftarrows Sem^+ + Sem^+ + BH$; Red is the reduced, Ox^{2+} the oxidized, and Sem^+ is the semireduced form of the redox system. The kinetics of the cross reactions, ${}_1Red + {}_2Ox^{2+} \rightleftarrows {}_1Sem^+ + {}_2Sem^+$, have also been measured for the pairs I(Red) + III(Ox^{2+}) and II(Red^{2-}) + III(Ox^{2+}) where II is 1-ethyl-2-quinolone-6-sulfonate azine. The rate and equilibrium constants correlate very well with the Marcus theory. The observation and/or absence, respectively, of concerted general acid–base catalysis is discussed by using More O'Ferral's and Jencks' method of estimating the free-energy surface of the system based on the free energies of the four corners of the contour map. Concerted catalysis is observed when the free energies of the two unstable intermediates are similar and high compared with the reactants and/or when the activation barrier for the electron transfer is very low which leads to enforced concerted catalysis.

Azaviolenes are a class of compounds which can exist in three different oxidation states, with the general structures shown.[2] Electron transfer from one state of another can occur

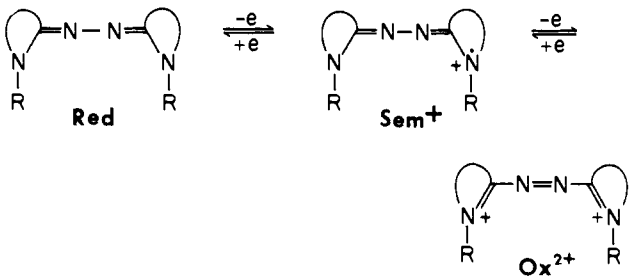

by the comproportionation–disproportionation reaction 1.

$$\text{Red} + Ox^{2+} \underset{k_{-1}}{\overset{k_1}{\rightleftharpoons}} 2Sem^+ \qquad (1)$$

In the first part of this series[1] we reported a kinetic study of the comproportionation–disproportionation of the systems derived from 1-ethyl-2-quinolone azine (I) and 1-ethyl-2-quinolone-6-sulfonate azine (II) in 50% 2-methoxyethanol–50% water (v/v) (ME–H_2O). Owing to the protonation of Red[3] on the bridge nitrogens,[4] to form $RedH^+$ [3] and $RedH_2^{2+}$,[3] two additional electron-transfer pathways had to be considered as shown in Scheme I. The rate law showed that for I all three pathways are significant, whereas for II only the two pathways k_1–k_{-1} and k_2–k_{-2} were detectable. Furthermore, the rate was found to be dependent on buffer concentration, suggesting a general acid–base catalyzed pathway:

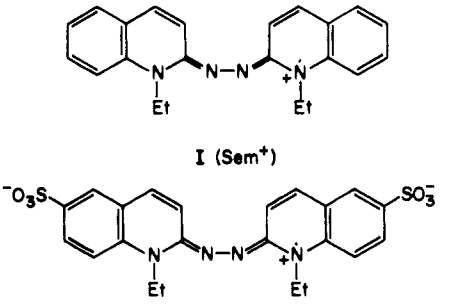

Scheme I

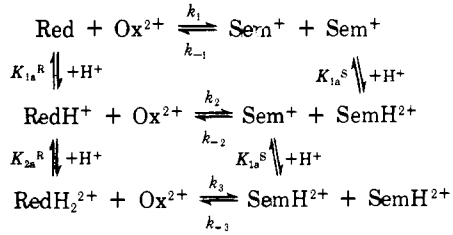

$$RedH^+ + Ox^{2+} + B^- \underset{k_{-2}^{BH}}{\overset{k_2^B}{\rightleftharpoons}} Sem^+ + Sem^+ + BH \qquad (2)$$

We have now extended this work to the systems derived from 1-ethyl-2-pyridone azine (III) and 1,3-dimethyl-2-benzimidazolone azine (IV), and also by measuring the cross reactions

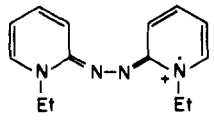

III (Sem$^+$)

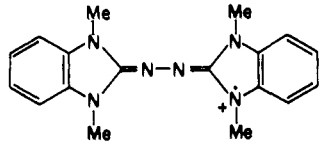

IV (Sem$^+$)

(eq 3) for the combinations I(Red) + III(Ox^{2+}) and II(Red^{2-}) + III(Ox^{2+}).

$$ {}_1\text{Red} + {}_2\text{Ox}^{2+} \underset{k_{-1}^{12}}{\overset{k_1^{12}}{\rightleftharpoons}} {}_1\text{Sem}^+ + {}_2\text{Sem}^+ \qquad (3) $$

Due to decomposition reactions occurring in some systems in ME-H_2O, particularly with III, we changed to a 50% acetonitrile-50% water (v/v) (AN-H_2O) solvent. For comparison purposes we also reinvestigated I in this new solvent whereas IV could be studied in both solvents.

Two main objectives have prompted this work. One is the relationship between kinetics and thermodynamics of electron-transfer reactions, in view of the possible application of the Marcus theory.[5] The other is the attempt to understand the factors which govern incidence or absence of general acid-base catalysis.

Results

General Features. There are various ways by which the equilibrium kinetics (relaxation) of a system such as Scheme I can be studied. However, in order to keep the kinetic analysis on a mathematically manageable level, one needs to work under conditions which permit the linearizations of the rate equation.[6] We used three different approaches. Two are based on small perturbations of the system at equilibrium, either by means of a temperature jump or a small pH jump; the other is based on initiating the reaction by mixing Red with Ox^{2+} in the stopped-flow apparatus, and if necessary, evaluating only the last few percent of the relaxation curve, i.e., when the system is already close to the equilibrium state.

In Part I[1] it was shown that the proton-transfer equilibria are all much more rapidly established than the electron-transfer equilibria. Thus the reciprocal relaxation time is given by:[1]

$$ \frac{1}{\tau} = k' \left(\frac{[\text{Ox}^{2+}] + [\text{Red}]_{\text{tot}}}{Q_R} + \frac{4[\text{Sem}^+]_{\text{tot}}}{K_1 Q_S^2} \right) \qquad (4) $$

with

$$ k_1' = k_1 + k_2[\text{H}^+]/K_{1a}^R + k_3[\text{H}^+]^2/K_{1a}^R K_{2a}^R + k_2^B[\text{H}^+][\text{B}^-]/K_{1a}^R \qquad (5) $$

$$ Q_R = 1 + [\text{H}^+]/K_{1a}^R + [\text{H}^+]^2/K_{1a}^R K_{2a}^R \qquad (6) $$

$$ Q_S = 1 + [\text{H}^+]/K_{1a}^S = 1 + K_2[\text{H}^+]/K_1 K_{1a}^R \qquad (7) $$

$$ [\text{Red}]_{\text{tot}} = [\text{Red}] + [\text{RedH}^+] + [\text{RedH}_2^{2+}] \qquad (8) $$

$$ [\text{Sem}^+]_{\text{tot}} = [\text{Sem}^+] + [\text{SemH}^{2+}] \qquad (9) $$

where all concentrations refer to their equilibrium values and where $K_1 = k_1/k_{-1}$, $K_2 = k_2/k_{-2}$. For the systems of this study we found that $[\text{H}^+]/K_{1a}^S \ll 1$ under all conditions. Hence, we shall replace Q_S by 1 and $[\text{Sem}^+]_{\text{tot}}$ by $[\text{Sem}^+]$ in subsequent equations.

In the temperature-jump and pH-jump experiments we chose $[\text{Ox}^{2+}] = [\text{Red}]_{\text{tot}}$ so that eq 4 becomes:[1]

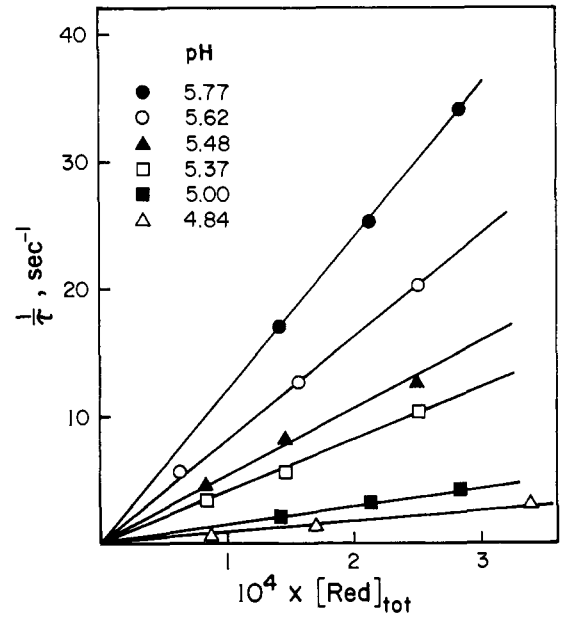

Figure 1. Representative stopped-flow data of system III in AN-H_2O, plots according to eq 11.

$$ \frac{1}{\tau} = k' \left(\frac{2}{Q_R\{2 + (K_1/Q_R)^{1/2}\}} + \frac{4(K_1/Q_R)^{1/2}}{K_1\{2 + (K_1/Q_R)^{1/2}\}} \right) \times [\text{Sem}^+]_0 \qquad (10) $$

where $[\text{Sem}^+]_0 = [\text{Red}]_{\text{tot}} + [\text{Ox}^{2+}] + [\text{Sem}^+]$.

In the experiments initiated by mixing Red with Ox^{2+} we chose $[\text{Red}]_{\text{tot}} \gg [\text{Ox}^{2+}]_0$. This is convenient because at the pH values where the equilibrium position favors the Sem^+ side, the relaxation time depends virtually only on the rates of the forward reactions, and thus $[\text{Red}]_{\text{tot}} \gg [\text{Ox}^{2+}]_0$ means pseudo-first-order conditions. This permits the entire relaxation curve to be evaluated, with a corresponding increase in precision. Here eq 4 becomes

$$ \frac{1}{\tau} = k' \left(\frac{1}{Q_R} + \frac{1}{\Phi} \right) [\text{Red}]_{\text{tot}} \qquad (11) $$

with

$$ \frac{1}{\Phi} = \frac{(K_1/Q_R)^{1/2}\{(K_1/Q_R) + 16/\gamma\}^{1/2} - K_1/Q_R}{K_1} \qquad (12) $$

where $\gamma = [\text{Red}]_{\text{tot}}/[\text{Ox}^{2+}]_0$. Pseudo-first-order conditions prevail as long as $1/Q_R \gg 1/\Phi$.

Plots of τ^{-1} vs. $[\text{Sem}^+]_0$ (eq 10) or vs. $[\text{Red}]_{\text{tot}}$ (eq 11) respectively provide straight lines with pH and buffer concentration dependent slopes. In conjunction with K_1, K_{1a}^R, and K_{2a}^R determined spectrophotometrically (see Experimental Section), the rate constants can be evaluated from these slopes.

All experiments were carried out at 25 °C, at a constant ionic strength, μ = 0.1 M (KCl). Buffer catalysis was only significant at concentrations >0.005 or >0.01 M. Thus data collected at buffer concentrations ≤0.01 M were fitted to eq 5 minus the $k_2^B[\text{H}^+][\text{B}^-]/K_{1a}^R$ term; these will be reported first. Throughout this paper we shall define $[\text{H}^+]$ as $10^{-\text{pH}}$.

Kinetics of III in AN-H_2O. In most runs we used the technique of mixing Ox^{2+} with a large excess of Red, but a number of experiments (see below) were performed by the pH-jump method. Typically, at any given pH value, τ^{-1} was measured at three different $[\text{Red}]_{\text{tot}}$, with $\gamma = [\text{Red}]_{\text{tot}}/[\text{Ox}^{2+}]_0 \geq 10$. Figure 1 shows some representative plots. From the slopes, $\tau^{-1}/[\text{Red}]_{\text{tot}}$, k' was obtained via eq 11 for 14 different pH values between pH 5.77 and 3.27. Table I[7] summarizes all the data.

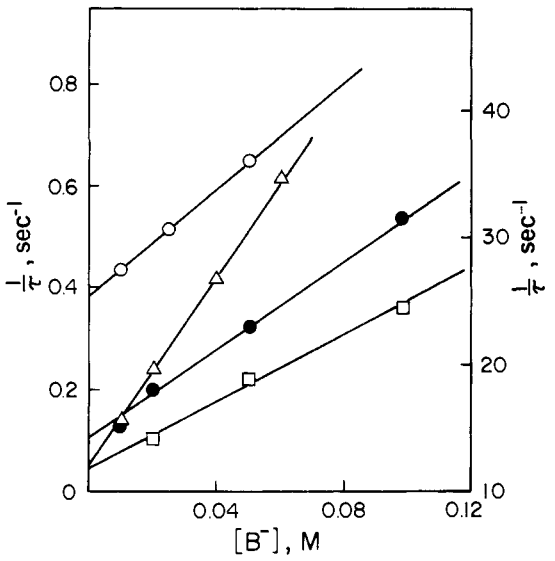

Figure 2. Representative plots of τ^{-1} vs. buffer base concentration in AN-H_2O. Open circles: III, $ClCH_2COO^-$, pH 4.51, $[Red]_{tot} = 1.85 \times 10^{-4}$ M, stopped-flow experiments, left ordinate scale; squares: III, $HCOO^-$, pH 4.00, $[Red]_{tot} = 3.07 \times 10^{-4}$ M, stopped-flow experiments, left ordinate scale; closed circles: III, CH_3COO^-, pH 5.56, $[Red]_{tot} = 2.55 \times 10^{-4}$ M, stopped-flow experiments, right ordinate scale; triangles: I, Cl_2CHCOO^-, pH 2.35, $[Sem^+]_0 = 8.23 \times 10^{-5}$ M, temperature-jump experiments, right ordinate scale.

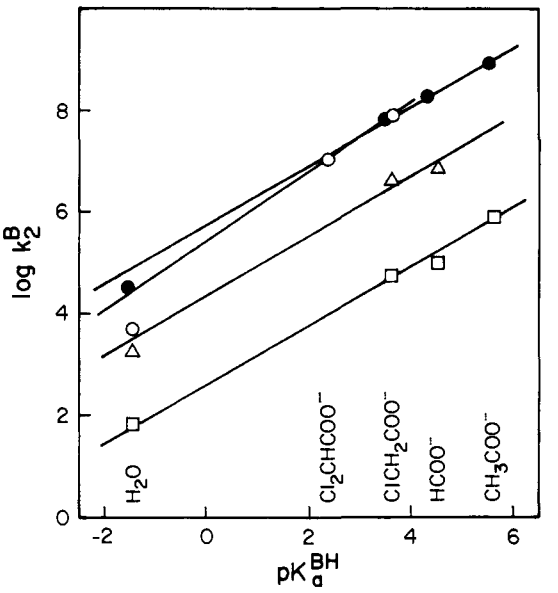

Figure 3. Bronsted plots for the general base catalyzed reaction $RedH^+ + Ox^{2+} + B^- \rightarrow 2Sem^+ + BH$. Data from Table VI, water reaction included (see Discussion). Open circles: I in AN-H_2O; closed circles: I in ME-H_2O (μ = 0.5 M, ref. 1); triangles: IV in AN-H_2O; squares: III in AN-H_2O.

A plot of k' vs. $[H^+]$, not shown, is linear, indicating that the $k_3[H^+]^2/K_{1a}{}^R K_{2a}{}^R$ term in eq 5 is insignificant in our pH range; from this plot k_1 and k_2 are obtained via the following equation ($K_{1a}{}^R$ is known):

$$k' = k_1 + k_2[H^+]/K_{1a}{}^R \qquad (13)$$

In the pH-jump experiments, k' was obtained from the slopes, $\tau^{-1}/[Sem^+]_0$, via eq 10. The results at six different pH values between pH 5.94 and 4.11 are summarized in Table II.[7] The two techniques gave the same results.

Kinetics of IV. IV was studied in both AN-H_2O and in ME-H_2O by using the stopped-flow mixing technique. The procedures were essentially the same as with III. The results (12 pH values between pH 3.96 and 0.98 in AN-H_2O; 11 pH values between pH 4.17 and 1.12 in 2-ME-H_2O) are summarized in Tables III[7] and IV.[7]

Kinetics of I in AN-H_2O. I was studied by the temperature-jump technique. The evaluation of the data was the same as that for the pH-jump experiments of III. The results at 13 different pH values between pH 3.99 and 1.03 are summarized in Table V.[7] It is noteworthy that k' can be fitted with eq 13; this contrasts with the situation in ME-H_2O where the $k_3[H^+]^2/K_{1a}{}^R K_{2a}{}^R$ term (eq 5) is significant at low pH values.[1]

General Acid-Base Catalysis. The dependence of τ^{-1} on buffer concentration was studied in several buffers. In our previous report[1] we have shown that buffer catalysis must represent acid-base catalysis rather than a specific salt effect. Plots of τ^{-1} vs. $[B^-]$, the concentration of the buffer base, at constant pH and constant $[Sem^+]_0$ or $[Red]_{tot}$ respectively afforded straight lines whose slopes permit the evaluation of $k_2{}^B$.[1] Typically three to four concentrations of B^-, in the range of 0.01 to 0.1 M, were used. Figure 2 shows four representative plots. Table VI summarizes the rate constants while Figure 3 shows Bronsted plots.

Kinetics of Cross Reactions (Eq 3). There is a potential problem with cross reactions in that a multitude of competing pathways may lead to a very complex reaction scheme. Scheme II, where only nonprotonated species are included, is the simplest version. However, if $K_1{}^{12} \ll K_1{}^{21}, K_1{}^{11}, K_1{}^{22} \gg 1$, the states **21, 11,** and **22** need not be considered and Scheme II reduces to eq 3. For the combination I(Red) + III(Ox^{2+}) where $K_1{}^{12} = 74$, $K_1{}^{21} = 8.50 \times 10^{11}$, $K_1{}^{11} = 8.80 \times 10^5$, $K_1{}^{22} = 7.15 \times 10^7$, and II($Red^{2-}$) + III($Ox^{2+}$) where $K_1{}^{12} = 3.58$, $K_1{}^{21} = 9.58 \times 10^{12}$, $K_1{}^{11} = 4.80 \times 10^5$, $K_1{}^{22} = 7.15 \times 10^7$, this is indeed the case;[8] $K_1{}^{12}$ was determined spectrophotometrically (see Experimental Section), while $K_1{}^{21}$ is found from $K_1{}^{21}K_1{}^{12} = K_1{}^{11}K_1{}^{22}$.

Scheme II

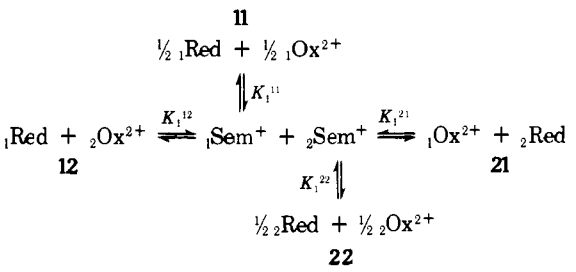

The kinetics were studied by the temperature-jump method. In order to keep states **11, 22,** and **21** of Scheme II insignificant, we could not work at very low pH values because this has the effect of shifting the equilibria away from the Sem^+ forms due to protonation of the Red forms. Thus, in the pH range studied, the data could be accommodated by Scheme III, i.e.,

Scheme III

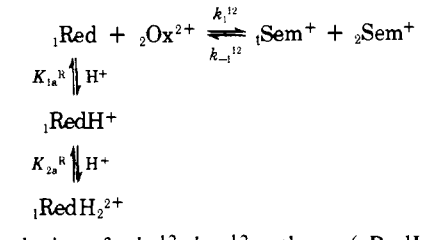

without inclusion of a $k_2{}^{12}$-$k_{-2}{}^{12}$ pathway ($_1RedH^+ + {}_2Ox^{2+} \rightleftarrows {}_1SemH^{2+} + {}_2Sem^+$). Also, and very noteworthy, no dependence on buffer concentration was found in a concentration range (0.01 to 0.06 M) where the other reactions show marked catalysis (Figure 2).

Table VI. Rate Constants for General Acid-Base Catalysis

BH		pK_a^{BH} [a]	k_2^B, $M^{-2}\,s^{-1}$	k_{-2}^{BH}, [b] $M^{-2}\,s^{-1}$
I in AN-H_2O	$ClCH_2COOH$	3.60	7.9×10^7	1.1×10^5
	$Cl_2CHCOOH$	2.35	1.1×10^7	2.7×10^5
	H_3O^+	−1.44 [c]	5.3×10^3 [d]	8.2×10^5 [d]
I in ME-H_2O [e]	CH_3COOH	5.50	7.8×10^8	4.8×10^4
	HCOOH	4.30	2.0×10^8	1.9×10^5
	$ClCH_2COOH$	3.55	7.6×10^7	4.1×10^5
	H_3O^+	−1.56 [f]	3.2×10^4 [d,g]	2.6×10^6 [d,g]
III in AN-H_2O	CH_3COOH	5.60	7.9×10^5	3.1×10^2
	HCOOH	4.52	1.0×10^5	4.8×10^2
	$ClCH_2COOH$	3.60	6.2×10^4	2.4×10^3
	H_3O^+	−1.44 [c]	6.4×10^1 [d]	2.8×10^5 [d]
IV in AN-H_2O	HCOOH	4.52	6.9×10^6	4.2×10^1
	$ClCH_2COOH$	3.60	4.4×10^6	2.2×10^2
	H_3O^+	−1.44 [c]	3.3×10^3 [d]	1.8×10^4 [d]

[a] Determined by potentiometric titration in the respective solvent. [b] $k_{-2}^{BH} = k_2^B K_a^{BH}/K_1 K_{1a}^R$. [c] $-\log [H_2O]$. [d] Assuming k_2 and k_{-2} refer to reaction 15 (see Discussion), $k_2^{H_2O} = k_2/[H_2O]$, $k_{-2}^{H_3O} = k_2/K_1 K_{1a}^R$. [e] Reference 1, $\mu = 0.5$ M. [f] $-\log([H_2O] + [ME])$. [g] Same assumption as *d*, but $k_2^{H_2O} = k_2/([H_2O] + [ME])$.

Table IX. Summary of Results [a]

	AN-H_2O					ME-H_2O	
	I	III	IV	I(Red) + III(Ox^{2+})	II(Red^{2-}) + III(Ox^{2+})	I [b]	IV
K_1	8.80×10^5	7.15×10^7	1.10×10^9	7.40×10^1 [c]	3.58 [c]	2.14×10^5	6.0×10^8
k_1 ($M^{-1}\,s^{-1}$)	4.98×10^9	2.52×10^9	8.29×10^9	1.45×10^9 [d]	1.81×10^9 [d]	1.82×10^9	2.5×10^9
k_{-1} ($M^{-1}\,s^{-1}$)	5.62×10^3	3.53×10^1	7.35	1.96×10^7 [e]	5.05×10^8 [e]	8.53×10^3	4.2
K_2	$\approx 9.0 \times 10^{-5}$	$\approx 5.0 \times 10^{-7}$	$\approx 4.5 \times 10^{-5}$	$\approx 7.6 \times 10^{-9}$ [f]	$\approx 3.5 \times 10^{-10}$ [g]	$\approx 9.0 \times 10^{-4}$	$\approx 2.0 \times 10^{-4}$
k_2 ($M^{-1}\,s^{-1}$)	1.47×10^5	1.78×10^3	9.24×10^4	$\approx 2.8 \times 10^1$ [h]		5.50×10^5	1.60×10^5
k_{-2} ($M^{-1}\,s^{-1}$)	$\approx 1.6 \times 10^9$	$\approx 3.6 \times 10^9$	$\approx 2.0 \times 10^9$	$\approx 3.7 \times 10^9$ [h]		$\approx 6.1 \times 10^8$	8.0×10^8
K_3	$\approx 2.7 \times 10^{-10}$	$\approx 5.2 \times 10^{-16}$	$\approx 2.2 \times 10^{-13}$	$\approx 3.6 \times 10^{-15}$ [i]		$\approx 6.9 \times 10^{-9}$	$\approx 7.0 \times 10^{-12}$
pK_{1a}^R	6.69	10.05	8.34	6.69	5.91	6.95	8.40
pK_{2a}^R	2.22	4.88	3.26	2.22	1.56	2.69	3.38
pK_{1a}^S	≈ -3.3	≈ -4.1	≈ -5.0			≈ -1.4	≈ -4.1
K_1/K_2	$\approx 9.8 \times 10^9$	$\approx 1.4 \times 10^{14}$	$\approx 2.5 \times 10^{13}$			$\approx 2.4 \times 10^8$	$\approx 3.0 \times 10^{12}$
K_1/K_3	$\approx 3.3 \times 10^{15}$	$\approx 1.4 \times 10^{23}$	$\approx 5.0 \times 10^{21}$			$\approx 3.1 \times 10^{13}$	$\approx 8.6 \times 10^{19}$

[a] All results at 25 °C, $\mu = 0.1$ M. [b] From reference 1. [c] K_1^{12}. [d] k_1^{12}. [e] k_{-1}^{12}. [f] K_2^{12}, obtained from $K_2^{12} = K_1^{12} K_{1a}^R/K_{1a}^S$ with K_{1a}^S of I($SemH^{2+}$). [g] $K_2^{12} = K_1^{12} K_{1a}^R/K_{1a}^S$ with K_{1a}^S of III($SemH^{2+}$). [h] From K_2^{12} and Figure 6. [i] $K_3^{12} = K_1^{12} K_{1a}^R K_{2a}^R/K_{1a}^{1S} \cdot K_{1a}^{2S}$.

The reciprocal relaxation time, under the conditions where $[_1Red]_{tot} = [_2Ox^{2+}]$ and $[_1Sem^+] = [_2Sem^+]$, is given by

$$\frac{1}{\tau} = k_1^{12} \times \left(\frac{1}{Q_R\{1 + (K_1^{12}/Q_R)^{1/2}\}} + \frac{(K_1^{12}/Q_R)^{1/2}}{K_1\{1 + (K_1^{12}/Q_R)^{1/2}\}} \right) \times [Sem^+]_0 \quad (14)$$

where $[Sem^+]_0 = [_1Red]_{tot} + [_2Ox^{2+}] + [_1Sem^+] + [_2Sem^+]$. Plots of $1/\tau$ vs. $[Sem^+]_0$ permit a determination of k_1^{12} from the slopes; the results are summarized in Tables VII[7] and VIII.[7]

Discussion

Table IX summarizes all equilibrium and rate constants (for the definition of rate constants and pK_a values see Schemes I and III; equilibrium constants are defined as $K_1 = k_1/k_{-1}$, $K_2 = k_2/k_{-2}$, etc.). K_1,[9] K_1^{12}, pK_{1a}^R,[9] pK_{2a}^R,[9] k_1, k_1^{12}, and k_2 were directly measurable and are known with good precision; so are $k_{-1} = k_1/K_1$ and $k_{-1}^{12} = k_1^{12}/K_1^{12}$.

The table also has entries for K_2, k_{-2}, and K_3; they were estimated by making the following assumptions. The first is that $SemH^{2+}$ is in fact an intermediate as shown in Scheme I. An alternative would be that $RedH^+ + Ox^{2+}$ are converted to $Sem^+ + Sem^+$ by the direct, presumably concerted, reaction

$$RedH^+ + Ox^{2+} + H_2O \underset{k_{-2}}{\overset{k_2}{\rightleftharpoons}} Sem^+ + Sem^+ + H_3O^+ \quad (15)$$

where H_3O^+ and H_2O act as general acid-base catalysts, in analogy to eq 2. Since our data could be fitted by assuming $Q_S = 1$ (eq 7) over the entire pH range, we have no direct evidence for the involvement of $SemH^{2+}$ and thus cannot distinguish between the two possibilities. However, in view of our previous study of I in ME-H_2O[1] where the rate law *did* prove[10] the involvement of $SemH^{2+}$, we shall assume the same to be true for the systems of the present study and assign k_2 and k_{-2} to the reactions shown in Scheme I. In the last section of the Discussion we shall come back to this point.

The second assumption is that one can apply the Marcus[5] theory (see next section) to our systems. Based on it one can calculate K_2 which correlates with a given k_2. Once K_2 is available, K_{1a}^S is accessible via the following equation:

$$K_{1a}^S = K_1 K_{1a}^R/K_2 \quad (16)$$

This then permits $K_3 = k_3/k_{-3}$ to be obtained from

$$K_3 = K_2 K_{2a}^R/K_{1a}^S = (K_2)^2 K_{2a}^R/K_1 K_{1a}^R \quad (17)$$

We believe that K_2 and K_{1a}^S thus estimated are reliable within

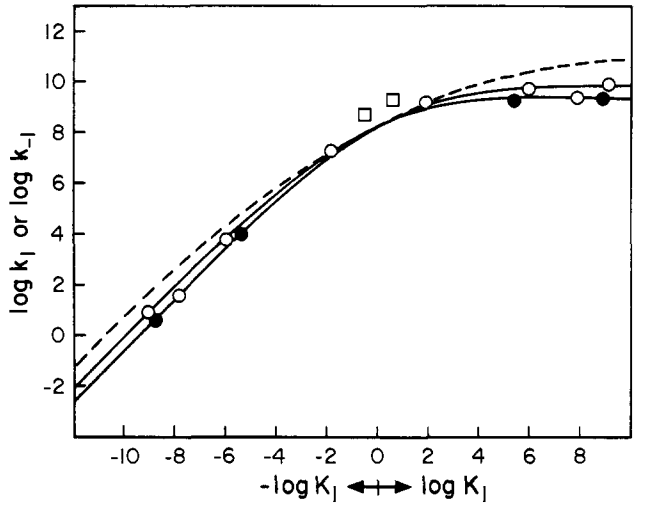

Figure 4. Log k_1 and log k_{-1} vs. log K_1. Open circles: reactions of charge type $++/0 \rightleftarrows +/+$, in AN-$H_2O$; closed circles, same but in ME-H_2O; squares: reaction of charge type $++/-- \rightleftarrows +/-$, in AN-$H_2O$. Dashed line: k_{act} based on eq 19; upper solid line: k_{obsd} from eq 18, with $k_{diff} = 7.7 \times 10^9$ M^{-1} s^{-1} in AN-H_2O; lower solid line: k_{obsd} from eq 18, with $k_{diff} = 2.5 \times 10^9$ M^{-1} s^{-1} in ME-H_2O.

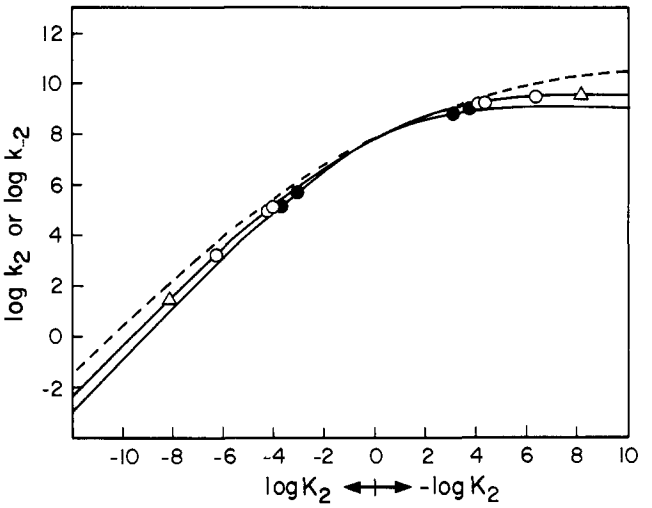

Figure 5. Determination of K_2 from experimental k_2 and Marcus curves. Dashed line: k_{act} based on eq 19; upper solid line: k_{obsd} from eq 18, with $k_{diff} = 3.85 \times 10^9$ M^{-1} s^{-1} in AN-H_2O; lower line: k_{obsd} from eq 18 with $k_{diff} = 1.25 \times 10^9$ M^{-1} s^{-1} in ME-H_2O.

a factor of 3 or better, K_3 within a factor of 9 (square dependence on K_2, eq 17). Despite these error limits, these estimates of K_2 and K_{1a}^S will be very useful in discussing the problem of concerted vs. stepwise catalysis (see below).

Rate vs. Equilibrium Constants. Correlation with Marcus Theory. According to the Marcus theory the observed rate constant of an electron-transfer reaction is given by

$$k_{obsd} = k_{act}k_{diff}/(k_{act} + k_{diff}) \quad (18)$$

where k_{diff} is the diffusion rate constant and k_{act} refers to the actual electron-transfer step; it is given by

$$k_{act} = Ze^{-\Delta G^*/RT} \quad (19)$$

where $Z = 10^{11}$ M^{-1} s^{-1} and ΔG^* is the free energy of activation. The theory calls for a relation between ΔG^* and the standard free energy of the reaction, $\Delta G°$, given by

$$\Delta G^* = \frac{W_r + W_p}{2} + \frac{\lambda}{4} + \frac{\Delta G°}{2} + \frac{(\Delta G° + W_p - W_r)^2}{4\lambda} \quad (20)$$

where W_r and W_p are Coulombic work terms for bringing reactants, respectively products, together; λ is a "reorganization parameter", given by

$$\lambda = \left(\frac{1}{2a_1} + \frac{1}{2a_2} - \frac{1}{r}\right)\left(\frac{1}{\epsilon_{op}} - \frac{1}{\epsilon_s}\right)(\Delta ze)^2 \quad (21)$$

where a_1 and a_2 are the effective radii of the reactants, r is the effective radius of the activated complex, usually taken as $a_1 + a_2$; ϵ_{op} is the optical dielectric constant, equal to the square of the refractive index; ϵ_s is the (static) dielectric constant; Δz is the number of electrons transferred; e is the charge of an electron.[11]

In Part 1[1] we have correlated our data with the Marcus equation by the following semiempirical method. By means of eq 19 ΔG^* was calculated for k_2 in the reaction of I in ME-H_2O and then eq 20 was solved for λ after assuming $W_r = W_p = 0$; with the resulting λ = 23,6 kcal/mol a Marcus curve of k_{act} vs. log K was constructed from eq 20 and 19, again assuming $W_r = W_p = 0$. Most experimental data points had a positive deviation from the curve, implying that our λ was too high. However, the points with the largest deviations referred to systems different from azaviolenes, studied under different conditions of temperature, solvent, and ionic strength. Thus no definite conclusions were possible.

The present data now show clearly that λ must be substantially lower; the reason why we obtained a high λ in our earlier work must be due to a too high K_2 value.[12] The new λ was estimated on the basis of the k_1^{12}-k_1^{12} (cross reactions, Scheme III) pairs as follows. Because $\Delta G°$ is close to zero, eq 20 can be simplified to

$$\Delta G^* = \frac{W_r + W_p}{2} + \frac{\lambda}{4} + \frac{\Delta G°}{2} \quad (22)$$

If we call W_o the work of bringing together two ions of equal unit charge, then $W_r = 0$ and $W_p = W_o$ for the system I(Red) + III(Ox^{2+}) with $(W_r + W_p)/2 = W_o/2$, and $W_r = -4W_o$ and $W_p = -W_o$ for the system II(Red^{2-}) + III(Ox^{2+}) with $(W_r + W_p)/2 = -5W_o/2$. Solving the two resulting simultaneous equations 22 for λ and W_o affords λ = 14.4 kcal/mol and W_o = 0.34 kcal/mol in AN-H_2O; incidentally, this λ corresponds to a = 6.77 Å.

By means of the appropriate form of eq 20, in combination with eq 19, log k_{act} vs. log K curves can then be constructed for the K_1 and K_2 equilibria. They are shown as dashed lines in Figures 4 and 5. In using these further we shall assume that they are the same in both solvents.[13]

From these curves one now obtains log k_{obsd} vs. log K by applying eq 18. In estimating k_{diff} for the k_1 reactions we used the Smoluchowski-Einstein-Stokes[16] expression, $k_{diff} = 8RT/3000\eta$, where η is the viscosity; it gives $k_{diff} = 7.7 \times 10^9$ M^{-1} s^{-1} in AN-H_2O (η = 0.08 P)[15] and 2.5×10^9 M^{-1} s^{-1} in ME-H_2O ($\eta \approx 0.026$ P).[15] For the k_2 reactions we assumed that the net effect of electrostatic repulsion minus the compensating effect of the high ionic strength leads to a twofold reduction of k_{diff}, thus $k_{diff} = 3.85 \times 10^9$ M^{-1} s^{-1} in AN-H_2O, 1.25×10^9 M^{-1} s^{-1} in ME-H_2O. The various log k_{obsd} vs. log K curves are shown in Figures 4 and 5 (solid lines).

It is apparent that the k_1-k_{-1} data fit very well with the calculated curves. In fact, for I and IV the points are virtually *on* the appropriate curve in both solvents and only slightly below it for III.[17] In view of this excellent fit we believe that the K_2 values can be fairly reliably estimated from the corresponding experimental k_2 values and the appropriate log k_{obsd} vs. log K curves in Figure 5.

Effect of Structure on Electron-Transfer Equilibria. A discussion of how K_1, K_2, and K_3 change with structure must consider the effect on the free energy of each species involved in a given equilibrium. Thus one cannot expect a simple relationship unless there is one factor which predominates. One

such factor which in certain cases may meet this criterion is resonance stabilization of Sem^+. Hünig et al.[4] have interpreted the much higher K_1 values for IV compared with I on the basis of better charge delocalization in the Sem^+ form of IV (four nitrogens) than of I (two nitrogens). On the other hand, the (perhaps naive) view that the quinoline moiety in I should be superior to the pyridine moiety in III in delocalizing the charge is not borne out in the K_1 values. However, the greater K_1 values for III compared with I is consistent with theoretical calculations by Čársky et al.[18]

The dependence of K_2 and K_3 on structure is not at all parallel to that of K_1. If resonance stabilization is accepted as being the main factor in determining structural effects on K_1, we may understand the K_2 and K_3 values as mainly reflecting the *loss* of this stabilization upon protonation of Sem^+. Thus, where this stabilization was greatest, the loss of it has the most dramatic effect which translates into large K_1/K_2 and K_1/K_3 ratios. These ratios are in fact much larger for III and IV compared with I. However, the near sameness of these ratios for III and IV shows that other factors also play a role.

General Acid–Base Catalysis. In all our systems except for the cross reactions, the rates are dependent on buffer concentration, indicating general acid–base catalysis. The rate constants for the catalyzed reactions are summarized in Table VI. Bronsted plots, shown in Figure 3, have slopes (β) between 0.58 and 0.68; these plots will be further discussed under the heading "Concerted H_2O/H_2O^+ Pathway?".

In our earlier report[1] we have shown that, among four possibilities, the most reasonable mechanism for general acid–base catalysis is that of eq 2; in view of the β values, a concerted type of catalysis appears the most likely.

A fairly widely accepted premise is that the primary reason for the existence of concerted general acid–base catalysis is that it avoids highly unstable intermediates and the high-energy transition states leading to them. Free-energy contour maps have become an increasingly popular tool for visualizing and discussing the problem.[19-22] Applied to our systems, the four corners of the contour map would be represented by the standard free energies of the four states labeled Reac (reactants), Prod (products), Int_1 (intermediate 1), and Int_2 (intermediate 2) in Scheme IV.

Scheme IV

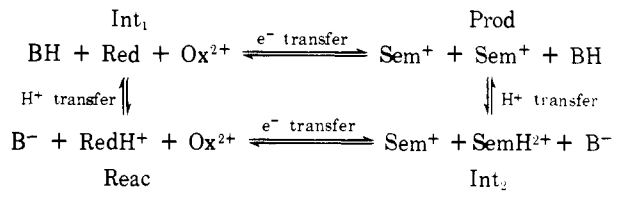

Two limiting situations are of particular interest. In the first, one of the intermediates, say Int_2, is of much higher energy than the other. In this case the preferred pathway is the stepwise process Reac → Int_1 → Prod whereas the pathway Reac → Int_2 → Prod is strongly disfavored.[23] Furthermore, the concerted pathway is also disfavored. This is a consequence of the shape of the free-energy surface; a schematic representation of a cross section through the surface along the Int_1–Int_2 axis is shown in Figure 6.[24] The reaction coordinate lies in the deepest valley of the surface which in this case goes through Int_1. If the high-energy intermediate is Int_1 instead of Int_2, the whole situation is simply reversed.

The second limiting situation is the one where the free energies of the intermediates are the same. Here the free-energy surface has a valley going through the middle as indicated by the cross section through the Int_1–Int_2 axis shown in Figure 6; this valley represents the concerted pathway which here is favored over the stepwise pathways.[25]

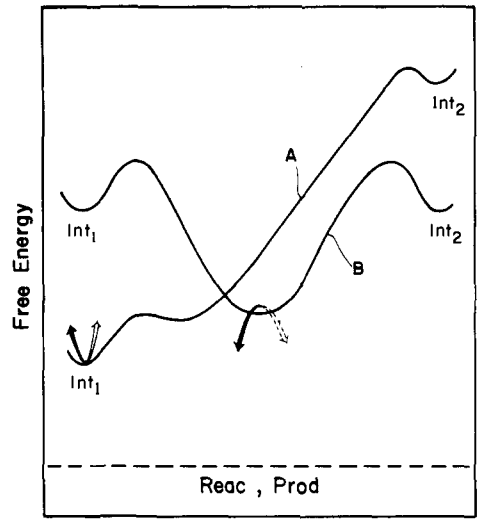

Figure 6. Schematic cross sections along Int_1–Int_2 axis of free-energy surface for Scheme IV. Energy levels of reactants and products assumed to be equal, dashed line. Double arrows indicate reaction coordinate. A: Energy of Int_2 much higher than energy of Int_1, reaction proceeds through Int_1; B: Int_1 and Int_2 are of same energy, reaction proceeds by concerted pathway through center of diagram.

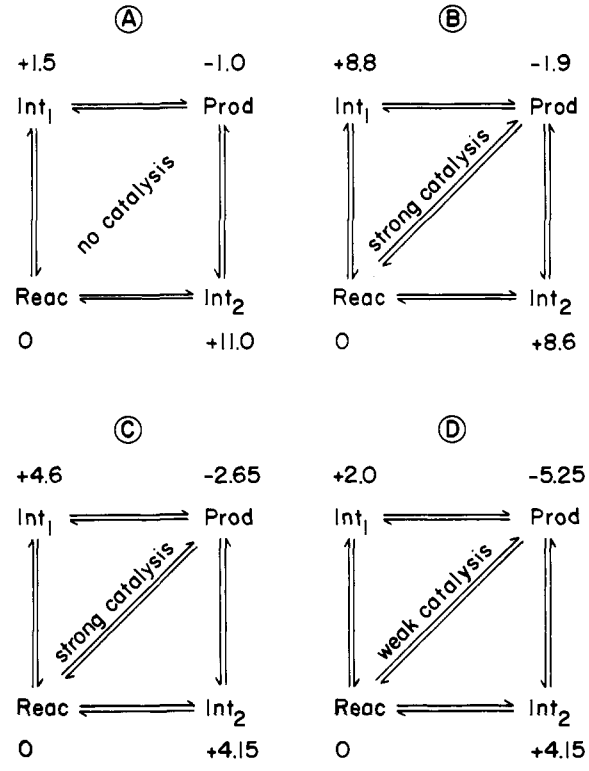

Figure 7. Standard free energies, in kcal/mol, of the four states in Scheme IV. $\Delta G°$ (Reac → Int_1) and $\Delta G°$ (Int_2 → Prod) defined as RT ln (K_{1a}^R/K_a^{BH}) and $-RT$ ln (K_{1a}^S/K_a^{BH}), respectively. A: cross reaction I(Red) + III(Ox^{2+}), acetate, in AN–H_2O; B: III, chloroacetate, in AN–H_2O; C: I, chloroacetate, in ME–H_2O; D: I, acetate, in ME–H_2O.

Three interesting questions immediately suggest themselves. (a) Since the concerted reaction is entropically disfavored, how unstable must the intermediates (assumed to be of about the same energy) be in order for the concerted pathway to become competitive? (b) If Int_1 and Int_2 are not equal in energy, how unequal do they have to get for the stepwise processes to become more favorable than the concerted mechanism? (c) Do the answers to (a) and (b) depend on the *activation* barriers for the various steps of the stepwise pathways?

Scheme V

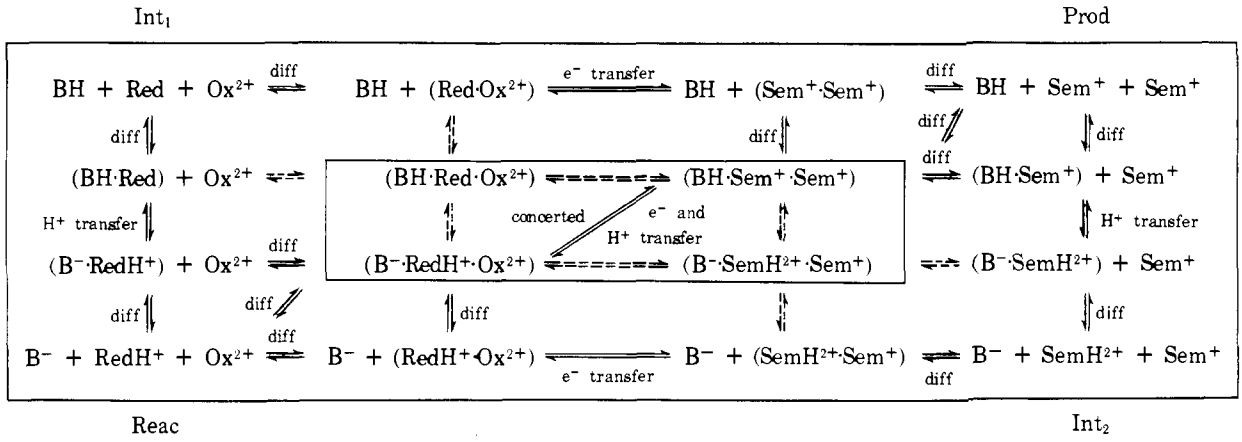

The systems of this study are particularly useful in shedding some light on these questions because in most of them all three pathways can be observed concurrently. In Figure 7 the corners of the contour maps for some typical cases, representing various limiting situations, are shown. The numbers are free energies in kcal/mol with the reactants chosen as reference state.

It appears that of the four cases represented in Figure 7, A and B can be interpreted in terms of the expectations based on Figure 6. Figure 7A refers to the cross reaction I(Red) + III(Ox^{2+}) in an acetate buffer, in AN-H_2O. No concerted catalysis was observed which is consistent with the large energy difference between Int_1 and Int_2 (curve A in Figure 6). Figure 7B represents system III in a chloroacetate buffer in AN-H_2O. Here Int_1 and Int_2 are of about equal energy and fairly high compared with Reac and Prod, a situation conducive to concerted catalysis (curve B in Figure 6). Concerted catalysis is observed; it is very efficient, e.g., at pH = pK_a^{BH} and $[B^-]$ = 1 M, the relative rates of the pathways (Reac → Prod):(Reac → Int_1 → Prod):(Reac → Int_2 → Prod) = 34.9:0.503:1.[26]

In the case C of Figure 7 (system I in a chloroacetate buffer in ME-H_2O) and even more so in case D (system I in an acetate buffer in ME-H_2O), the observation of concerted catalysis is surprising because the energy of the intermediates relative to reactants is not very high. In case C catalysis is even more efficient than in case B, e.g., at pH = pK_a^{BH} and $[B^-]$ = 1 M, the relative rates of the pathways (Reac → Prod):(Reac → Int_1 → Prod):(Reac → Int_2 → Prod) = 104:1:0.76.[26] In case D it is less efficient but still significant, with a ratio of 7.35:1:0.0107[26] for the respective pathways.

These results suggest that another factor plays an important role. It can be illustrated by considering the extended Scheme V which includes the various encounter complexes (species in parentheses). In this scheme the k_1-k_{-1} process corresponds to the top line where the first and the last steps are diffusional processes whereas the step (Red·Ox^{2+}) ⇌ (Sem^+·Sem^+) refers to the actual electron transfer with the rate constant k_{act} (eq 18 and 19). Similarly the k_2-k_{-2} process is represented by the bottom line. The concerted process, (B^-·$RedH^+$·Ox^{2+}) ⇌ (BH·Sem^+·Sem^+) is also seen to be preceded and followed by diffusional steps for which there are different possibilities.

Let us now consider the idealized situation where the energy of Int_1 relative to Reac is constant but where K_1 increases from one system to another. When K_1 is small, the activation barrier, ΔG^*, for the process (Red·Ox^{2+}) → (Sem^+·Sem^+) is relatively high, making k_{act} (eq 19) relatively small and thus the rate-limiting factor in the k_1 step (eq 18). A relatively large ΔG^* also implies an even higher activation barrier for the process (B^-·$RedH^+$·Ox^{2+}) → (BH·Sem^+·Sem^+) which leads to a rather small k_2^B. This is essentially the situation with the cross reactions where the concerted pathway is too slow to compete with the stepwise reaction; these considerations thus provide an alternative interpretation for the absence of buffer catalysis in the cross reactions.

If K_1 is increased, ΔG^* decreases; this also reduces the activation barrier of the process (B^-·$RedH^+$·Ox^{2+}) → (BH·Sem^+·Sem^+). As a consequence k_2^B increases; on the other hand k_1 remains relatively unaffected because once k_1 is close to the diffusion-controlled limit, a reduction in ΔG^* has little effect on k_1. Thus the relative importance of the concerted compared with the stepwise pathway increases and buffer catalysis becomes observable. This then represents an example of enforced concerted catalysis[27] which is a consequence of low activation barriers for the electron-transfer process.

Concerted H_2O/H_3O^+ Pathway? In our analysis we have assumed throughout that k_2 and k_{-2} refer to the reaction shown in Scheme I instead of reaction 15. However, it is possible that both reactions occur concurrently because of enforced concerted catalysis as in the buffer reactions, due to low activation barriers of the processes ($SemH^{2+}$·Sem^+) → ($RedH^+$·Ox^{2+}) and (H_3O^+·Sem^+·Sem^+) → (H_2O·$RedH^+$·Ox^{2+}). Concurrent mechanisms of the water reaction are not without precedent[28] but the question cannot be answered unequivocally in the present case.

A positive deviation of the water point from the Bronsted plot is sometimes taken as evidence that the water reaction proceeds by a different mechanism than the buffer reaction.[20] We have included the water points in our Bronsted plots. For I in AN-H_2O, the water point deviates negatively from the line by approximately 0.7 log unit, for the same system in ME-H_2O and for III in AN-H_2O it is almost on the line. For IV there are insufficient data to be sure, but assuming the same slope (β) as for III, the water point appears to be very near the line too.

These observations are difficult to interpret because one has to take into account that the reactions which define the Bronsted lines involve negatively charged bases; this is expected to have a substantial accelerating effect compared with the electrostatically unfavorable water reactions.[29] Thus one might be tempted to interpret the fact that for I the water point moves up when changing from AN-H_2O to ME-H_2O because of the much higher ionic strength used in the latter solvent (μ = 0.5 M instead of 0.1 M). Such an interpretation would also imply that the water points of III and IV should actually lie above the line, if it were not for the charge effect, consistent with the assumption that the stepwise mechanism for the water reaction is predominant. Even though these arguments seem reasonable, no definite conclusions should be drawn from these considerations.

It should be noted that if the concerted reaction 15 does significantly contribute to k_2, our estimates of K_2 and with it

those of pK_{1a}^{S} and K_3 may be somewhat too high, while the free energy of Int_2 in Figure 7 would be somewhat too low, however, without changing the qualitative picture.[30]

Experimental Section

Materials. Water, 2-methoxyethanol, and chloroacetic acid were purified as described in Part 1.[1] Reagent grade acetic acid, dichloroacetic acid, formic acid (88%), potassium hydrogen phthalate, potassium dihydrogen phosphate, citric acid, borax, and sodium chloride were used without further purification. The azaviolenes I and II in their various oxidation states were available from our previous study[1] whereas III and IV were generously supplied by Professor S. Hünig.

pH Measurement and pK_a Determinations. The pH measurements were carried out as described previously,[1] and $[H^+]$ was defined as 10^{-pH}. The pK_{1a}^{R} and pK_{2a}^{R} values were determined by the standard spectrophotometric procedure of measuring absorbance at five to seven different pH values and applying the following equations:

$$pK_{1a}^{R} = pH + \log \frac{A_{Red} - A}{A - A_{RedH^+}} \quad (23)$$

$$pK_{2a}^{R} = pH + \log \frac{A_{RedH^+} - A}{A - A_{RedH^{2+}}} \quad (24)$$

where A is the absorbance at a pH near the pK, A_{red} the absorbance at high pH when Red is completely in the unprotonated form, etc. The following wavelengths and buffers were used: λ 450 nm and sodium dihydrogen phosphate for pK_{1a}^{R} of I; λ 350 nm and HCl for pK_{2a}^{R} of I; λ 450 nm and acetate or sodium dihydrogen phosphate for pK_{1a}^{R} of II; λ 420 nm and HCl for pK_{2a}^{R} of II; λ 320 nm and borax or sodium dihydrogen phosphate for pK_{1a}^{R} of III; λ 365 nm and potassium hydrogen phthalate for pK_{2a}^{R} of III; λ 347 nm and sodium dihydrogen phosphate for pK_{1a}^{R} of IV; λ 322 nm and citrate for pK_{2a}^{R} of IV. In the case of II and III, decomposition of Red sets in at pH >6 and pH >8, respectively, which necessitates to use only freshly prepared solutions and to work very fast.

K_1 and K_1^{12} Determinations. K_1 and K_1^{12} were determined spectrophotometrically. For K_1, solutions were prepared by dissolving Sem^+ in the appropriate buffer, while for K_1^{12} the solutions were made by dissolving equal molar amounts of ${}_1Red$ and ${}_2Ox^{2+}$. The constants were found from eq 25[31] and 26, respectively:

$$K_1 = 4Q_R \left(\frac{A_{Ox^{2+}} - A}{A - A_{Sem^+}}\right)^2 \quad (25)$$

$$K_1^{12} = Q_R \left(\frac{A_{Ox^{2+}} - A}{A - A_{Sem^+}}\right)^2 \quad (26)$$

in eq 25, $A_{Sem^+} = \epsilon_{Sem^+}[Sem^+]_0$ and $A_{Ox^{2+}} = 0.5\epsilon_{Ox^{2+}}[Sem^+]_0$; in eq 26, $A_{Sem^+} = (\epsilon_{1Sem^+} + \epsilon_{2Sem^+})[{}_2Ox^{2+}]_0$ and $A_{Ox^{2+}} = \epsilon_{Ox^{2+}}[{}_2Ox^{2+}]_0$. These equations hold only at wavelengths where Red, $RedH^+$, and $RedH_2^{2+}$ do not absorb. Typically, determinations were made on five to seven solutions of different pH. The following wavelengths, buffers and pH ranges were used: λ 520 nm, HCl, pH 1.78–2.53 for I; λ 560 nm, formate and chloroacetate, pH 3.64–4.65 for III; λ 385 nm, HCl, pH 1.38–2.35 for IV; λ 525 nm, HCl, pH 1.24–1.74 for II; λ 520 nm, acetate, pH 4.19–5.74 for I(Red) + III(Ox^{2+}); λ 520 nm, acetate and chloroacetate, pH 3.76–5.18 for II(Red^{2-}) + III(Ox^{2+}).

Kinetic Measurements. The temperature-jump and stopped-flow experiments were carried out as described previously.[1] In the pH-jump experiments, the pH-jump was produced by mixing, in the stopped-flow apparatus, a weakly buffered reaction solution with a more strongly buffered reaction solution of different pH.

Acknowledgment is made to the donors of the Petroleum Research Fund, administered by the American Chemical Society, for the support of this research. We also thank Professor W. P. Jencks for discussion and criticism of the manuscript.

Supplementary Material Available: Tables I–V, VII, and VIII summarizing all experimental data on the relaxation times (7 pages). Ordering information is given on any current masthead page.

References and Notes

(1) Part 1: C. F. Bernasconi, R. G. Bergstrom, and W. J. Boyle, Jr., *J. Am. Chem. Soc.* **96**, 4643 (1974).
(2) S. Hünig, *Pure Appl. Chem.*, **15**, 109 (1967).
(3) Note that for II all species have a net charge reduced by two, e.g., Sem^-, Red^{2-}, $RedH^-$, Ox, etc.
(4) S. Hünig, H. Balli, H. Conrad, and A. Schott, *Justus Liebigs Ann. Chem.*, **676**, 52 (1964).
(5) (a) R. A. Marcus, *J. Chem. Phys.*, **24**, 966 (1956); (b) *ibid.*, **43**, 679, 3477 (1965); (c) *Discuss. Faraday Soc.*, **29**, 21 (1960); (d) *J. Phys. Chem.*, **67**, 853 (1963).
(6) C. F. Bernasconi, "Relaxation Kinetics", Academic Press, New York, N.Y., 1976, pp 3, 63, 81.
(7) See paragraph concerning supplementary material at the end of this paper.
(8) In finding the right combination we were guided by the known[4] oxidation–reduction potentials of the various species.
(9) Hünig et al.[4] have measured K_1, pK_{1a}^{R}, and pK_{2a}^{R} for I and IV in Me–H_2O by a polarographic method. The agreement between their and our values is satisfactory but not perfect; the discrepancies are too small to warrant discussion.
(10) Evidence for the involvement of $SemH^{2+}$ can be based on $Q_S > 1$, or, if $Q_S = 1$, on the presence of a $k_3[H^+]^2/K_{1a}^{R}K_{2a}^{R}$ term (eq 5). This latter must arise either from the reaction indicated in Scheme I, or perhaps from the concerted process $RedH_2^{2+} + Ox^{2+} + H_2O \rightleftarrows Sem^+ + SemH^{2+} + H_3O^+$; the tetramolecular process $RedH_2^{2+} + Ox^{2+} + 2H_2O \rightleftarrows 2Sem^+ + 2H_3O^+$ is extremely unlikely on entropy grounds. The data for I in ME–H_2O[1] suggested that both $Q_S > 1$ and that there is a $k_3[H^+]^2/K_{1a}^{R}K_{2a}^{R}$ term; the best fit was obtained with $pK_{1a}^{S} = 0.18$ and $k_3 = 2.7 \times 10^3\ M^{-1}\ s^{-1}$ at $\mu = 0.5$ M. However, the fit was not very sensitive to some increase in k_3 with a corresponding decrease in pK_{1a}^{S} and thus the reported values may not be very accurate. The data of the present study, in fact, suggest that pK_{1a}^{S} is lower and with it K_2 than previously reported (Table IX).
(11) $e = 4.80 \times 10^{-10}$ esu; λ obtained is in erg/molecules and needs to be converted to desired units, e.g., kcal/mol.
(12) As pointed out in ref 10, the curve fitting of the data was not very sensitive to changes in K_2.
(13) Assuming the same radii in both solvents, eq 21 permits one to obtain $\lambda_{ME-H_2O} = \lambda_{AN-H_2O}(\epsilon_{op}^{-1} + \epsilon_s^{-1})_{ME-H_2O}/(\epsilon_{op}^{-1} + \epsilon_s^{-1})_{AN-H_2O} = 13.63$ kcal. This small reduction is expected to be roughly compensated by a small increase in W_o due to a somewhat lower ϵ_s.[14]
(14) $\epsilon_{op} = n^2 = (1.346)^2$ in AN–H_2O,[15] $(1.3804)^2$ in ME–H_2O;[1] $\epsilon_s = 58.7$ in AN–H_2O,[15] 52.0 in ME–H_2O.[15]
(15) G. J. Janz and R. P. T. Tomkins, "Nonaqueous Electrolyte Handbook", Vol. 1, Academic Press, New York, N.Y., 1972.
(16) E. F. Caldin, "Fast Reactions in Solution", Wiley, New York, N.Y., 1964, p 10.
(17) Note that since the cross reaction I(Red) + III(Ox^{2+}) is of the same charge type as the K_1 equilibria, the respective k_1^{12} and k_{-1}^{12} points are (by definition) exactly on the dashed (log k_{act}) curve. On the other hand, for the cross reaction II(Red^{2-}) + III(Ox^{2+}), the points deviate (by definition) by 0.76 log unit, corresponding to 1.04 kcal/mol or $3W_o$.
(18) P. Čársky, S. Hünig, D. Scheutzow, and P. Zahradnik, *Tetrahedron*, **25**, 4781 (1969).
(19) R. A. More O'Ferral, *J. Chem. Soc. B*, 274 (1970).
(20) W. P. Jencks, *Chem. Rev.*, **72**, 705 (1972).
(21) B. M. Dunn, *Int. J. Chem. Kinet.*, **6**, 143 (1974).
(22) T. C. Bruice, *Prog. Bioorg. Chem.*, **4**, 1 (1976).
(23) This will be true unless the transition state of the step Reac → Int_1 or of step Int_1 → Prod is of very high energy, higher than Int_2 and the two transition states of the other stepwise pathway. In our systems neither proton nor electron transfers have high activation barriers.
(24) Whether there is indeed a relative minimum between Int_1 and Int_2 as drawn in the figure is not certain. However, this is immaterial to our discussion.
(25) Note that the pictorial representation of this situation is just another way to state the libido rule, W. P. Jencks, *J. Am. Chem. Soc.*, **94**, 4731 (1972); the rule states: "Concerted general acid–base catalysis of complex reactions in aqueous solution can occur only (a) at sites that undergo a large change in pK in the course of the reaction and (b) when this change in pK converts an unfavorable to a favorable proton transfer with respect to the catalyst, i.e., the pK of the catalyst is intermediate between the initial and final pK values of the substrate site".
(26) Relative rates taken as $k_2^{B}[B^-]$ for concerted reaction, $k_1K_{1a}^{R}/[H^+]$ for Reac → Int_1 → Prod pathway, k_2 for Reac → Int_2 → Prod pathway.
(27) W. P. Jencks, *Acc. Chem. Res.*, **9**, 425 (1976).
(28) See, e.g., S. Rosenberg, S. M. Silver, J. M. Sayer, and W. P. Jencks, *J. Am. Chem. Soc.*, **96**, 7986 (1974).
(29) A. J. Kresge and Y. Chiang, *J. Am. Chem. Soc.*, **95**, 803 (1973).
(30) For example, if there were a 50% contribution by the concerted pathway, the true k_2 values would be half of those reported, with K_2 reduced by roughly the same factor while pK_{1a}^{S} would be lowered by 0.3 unit and the free energies of Int_2 would be raised by 0.41 kcal/mol. In the rather unlikely event that the concerted reaction is as much as nine times more effective than the stepwise pathway, k_2 would be reduced tenfold, K_2 about eightfold, and pK_{1a}^{S} by 0.8 unit; the energies of all Int_2 would be raised by 1.1 kcal/mol.
(31) Equation 25 differs from that given in Part 1[1] because of a different definition of A_{Sem}.